Analyst

PAPER

View Article Online
View Journal | View Issue

Cite this: *Analyst*, 2014, **139**, 837

Effect of processing parameters for electrocatalytic properties of SnO_2 thin film matrix for uric acid biosensor

Kashima Arora,[a] Monika Tomar[b] and Vinay Gupta*[a]

Received 20th August 2013
Accepted 4th December 2013

DOI: 10.1039/c3an01582c

www.rsc.org/analyst

RF sputtered tin oxide (SnO_2) thin film matrix has been efficiently exploited for the detection of uric acid. The deposition parameters for SnO_2 thin film have been optimized to yield better electrocatalytic properties. A correlation between its electrocatalytic properties with the structural and electrical properties has been made. SnO_2 thin film prepared under optimized growth parameter (70% argon in reactive gas ambient of Ar and O_2) exhibits higher mobility of charge carrier and high carrier concentration thereby resulting in enhanced charge transfer characteristics. High surface coverage of uricase onto SnO_2 thin films (4.28×10^{-4} mole cm^{-2}), low value of Michaelis–Menten constant (k_m) 0.18 mM, good linearity in detection of uric acid in the range 0.05–1.00 mM and a fast response of 5 s are attractive features of prepared SnO_2 thin film based bioelectrodes for efficient detection of uric acid. The nanoporous and rough surface morphology of SnO_2 thin film besides its high carrier mobility in comparison to that of ITO is responsible for the obtained enhanced sensitivity (~700 μA mM^{-1}) and improved sensing response characteristics towards uric acid.

Introduction

In human beings, purines are degraded into uric acid which further degrades with the help of uricase to the ring of allantoin which is then excreted. However, in cases where purine degradation stops at the uric acid stage only, there can be problems, since in contrast to allantoin, uric acid is poorly soluble in water. Excessive concentrations of uric acid can develop in the blood (*hyperuricemia*) when its processing is disturbed, resulting in the accumulation of uric acid crystals in the body. Deposition of these crystals in the joints can cause very painful attacks of *gout*. Most cases of hyperuricemia are due to disturbed uric acid excretion *via* the kidneys or high purine diet (*e.g.*, meat). The normal level of uric acid in human blood is 0.15–0.45 mM (2.52–7.56 mg dl^{-1}). Consequently, determination of uric acid is of paramount importance in the diagnosis of the diseases caused by disorder of purine biosynthesis and catabolism. Amongst different approaches reported for the detection of uric acid levels, such as chemiluminescence,[1] flouroscence,[2] coulometric,[3] and enzymatic-spectrophotometric methods,[4] amperometric biosensors provide advantages like low cost instrumentation, improved sensitivity and selectivity, fast response, good reproducibility and long shelf life.

Since efficient immobilization of enzyme on a thin film matrix and its stability are important factors in the fabrication of biosensors, the search for suitable materials which may provide large surface area for higher enzyme loading and a compatible microenvironment that helps enzyme's bioactivity is thus of great importance. Various immobilization methods for biomolecules, such as physical adsorption,[5] entrapment,[6] cross-linking,[7] and covalent attachment,[8] have been utilized for the technological development of biosensors. Among these methods, the covalent binding of an enzyme with a supporting matrix, has an added advantage of stronger attachment resulting in reduced leaching out of the immobilized enzyme. Since the matrix plays a crucial role in the performance of a biosensor, various matrices have been explored including polymers, nanoparticles, metal oxide thin films, composite films, monolayers *etc.* Recently, metal oxide thin films have attracted the interest of the research community for biosensor applications due to their advantages including biocompatibility, low cost, good sensitivity, high selectivity, low detection limit *etc.* over other materials.[9–11] Different metal oxides have been used for developing uric acid biosensors, however, development of a suitable matrix for efficient immobilization of enzyme (uricase) and exhibiting enhanced response characteristics for uric acid is still lacking.[12,13] SnO_2 due to good electrocatalytic property and ease fabrication may provide a suitable platform for immobilization of uricase as compared to metal oxide matrices and further, development of SnO_2 thin film with porous morphology may provide additional advantages. However, very little attention has been given to exploring the biosensing properties of the SnO_2 thin film.[14,15]

[a]*Department of Physics and Astrophysics, University of Delhi, Delhi 110007, India. E-mail: vgupta@physics.du.ac.in*

[b]*Department of Physics, Miranda House, University of Delhi, Delhi 110007, India*

In the present work, uricase has been immobilized successfully on the surface of SnO_2 thin film by covalent bonding technique using cross linkers and a uric acid biosensor is developed. Structural and electrical properties of the SnO_2 thin film matrix have been studied and correlated with their electrocatalytic and charge transfer characteristics. The prepared uric acid biosensor exhibits the enhanced sensing response characteristics including high sensitivity, good linearity over a wide range of uric acid concentrations, fast response, high stability and long shelf life.

Experimental

Materials

Uricase (E.C. 1.7.3.3 from *Candida* sp.), horseradish peroxidase (HRP, 200 U mg^{-1}), *o*-dianisidine and uric acid were purchased from Sigma Aldrich. Amino propyl triethoxy silane (APTES) and potassium ferricyanide were procured from Merck (India). Sodium phosphate monobasic anhydrous and sodium phosphate dibasic dihydrate were obtained from Sisco Chemical, India. All chemicals were used without further purification. De-ionized water (18.2 Ω cm resistivity) was used in the preparation of aqueous solutions.

Preparation of solutions

Phosphate buffer saline (PBS) 50 mM, pH 7.0 (0.9% NaCl) solution was prepared by adjusting the proportion of monobasic sodium phosphate and dibasic sodium phosphate solutions and then adding 0.9% NaCl to the solution. Uricase (1 mg ml^{-1}) and HRP solutions (1 mg ml^{-1}) were freshly prepared in PBS buffer of pH 7.0. Different concentrations of uric acid solution and solution of *o*-dianisidine (1%) were freshly prepared in de-ionized water.

Preparation of SnO_2 thin film electrode

SnO_2 thin films were deposited by RF sputtering technique onto platinum (Pt) coated corning glass slides. Platinum (Pt) thin film of 100 nm thickness was deposited on corning glass substrate by RF sputtering technique under 100% Ar gas ambient using Pt metal target (99.99% pure) at a pressure of 10 mTorr. In order to improve the adhesion of Pt thin film on corning glass substrate, an ultra thin (~10 nm) buffer layer of titanium (Ti) was sputter coated prior to Pt deposition under the same deposition condition. SnO_2 thin film was deposited on Pt coated corning glass slide (SnO_2/Pt) to serve as a matrix for uric acid biosensor. A 4 inch diameter tin target (99.99% pure) is sputtered at an RF power of 150 W keeping the target to substrate distance fixed at 7.5 cm. The SnO_2 thin film of about 180 nm thickness was deposited at room temperature substrate under the processing pressure of 14 mTorr. Since the conductivity of SnO_2 thin film may play an important role in obtaining the charge transfer characteristics, the content of Ar gas in the reactive gas mixture (Ar + O_2) was varied from 30% to 80% in order to obtain different stoichiometry of SnO_2 thin film matrices. Commercially available ITO coated glass slide is also used as a matrix for comparison with SnO_2 thin films in obtaining enhanced response characteristics towards uric acid.

Preparation of SAM of APTES on SnO_2/Pt and ITO films and immobilization of uricase

The uricase enzyme is immobilized on the surface of SnO_2 and ITO thin film matrices using EDC/NHS chemistry to create covalent bonding between the NH_2 group of self assembled monolayer (SAM) of aminopropyltriethoxysilane (APTES) and COOH group of uricase. The hydrolysis of the prepared samples (SnO_2/Pt and ITO) were carried out by immersing in a solution of H_2O_2–NH_4OH–H_2O (1 : 1 : 5, v/v) for 30 min at 80 °C, and subsequently were rinsed thoroughly with de-ionized water and dried in a jet of dry N_2. The uniformly distributed OH groups were obtained on the surface of SnO_2/Pt and ITO electrodes after hydrolysis. The hydrolyzed SnO_2 and ITO film based electrodes were immersed in 1% (v/v) solution of APTES in toluene overnight at room temperature for silanization. After the coupling reaction, the electrodes were rinsed with toluene and water to remove the physically adsorbed silanes on its surface and a monolayer of APTES was obtained on the surface of SnO_2 and ITO based electrodes. The modified electrodes were dried under a stream of nitrogen. The uricase was covalently attached to APTES SAM using EDC/NHS chemistry as shown in the schematic in Fig. 1(a). Maximum binding of uricase enzyme was observed when 5 μl of uricase solution was diluted to 30 μl in distilled water containing 0.4 M EDC and 0.1 M NHS. The enzyme solution was poured onto a 1.0 cm^2 area of SnO_2 and ITO thin film based electrodes, respectively, and was kept for approximately 4 h in a humid chamber at room temperature for uricase (Ur) binding. The immobilization of uricase on electrode surface occurs *via* a coupling reaction between the amino group of silane and the EDC/NHS activated carboxylic group of uricase. The prepared bioelectrodes (Ur/SnO_2/Pt/Ti/glass and Ur/ITO/glass) were washed thoroughly with phosphate buffer (50 mM, pH 7.0) containing 0.9% NaCl to remove any unbound enzyme and was stored at 4 °C when not in use. The schematic of the prepared bioelectrodes (Ur/SnO_2/Pt/Ti/glass and Ur/ITO/glass) are shown in Fig. 1(b) and (c).

Measurement and apparatus

The structural, optical and electrical properties (resistivity, carrier concentration and mobility of charge carriers) of the prepared SnO_2 thin film and commercially available ITO film were studied using X-ray diffractometer (Bruker D8 Discover), double beam UV-Visible Spectrophotometer (Perkin Elmer, Lambda 35) and Hall effect measurement in Vander Pauw arrangement, respectively. Fourier transform infrared spectrophotometer (FTIR) (Perkin Elmer Model: Spectrum BX) was used to confirm the immobilization of uricase. The modification of surface morphology after the immobilization of the enzyme (uricase) of the prepared Ur/SnO_2/Pt/Ti/glass and Ur/ITO/glass bioelectrodes were investigated using atomic force microscope (Veeco DICP2) in non-contact mode and images were analyzed by SPM Lab Analysis software. Scanning Electron Microscopy (SEM) has been used to study the nanoporous

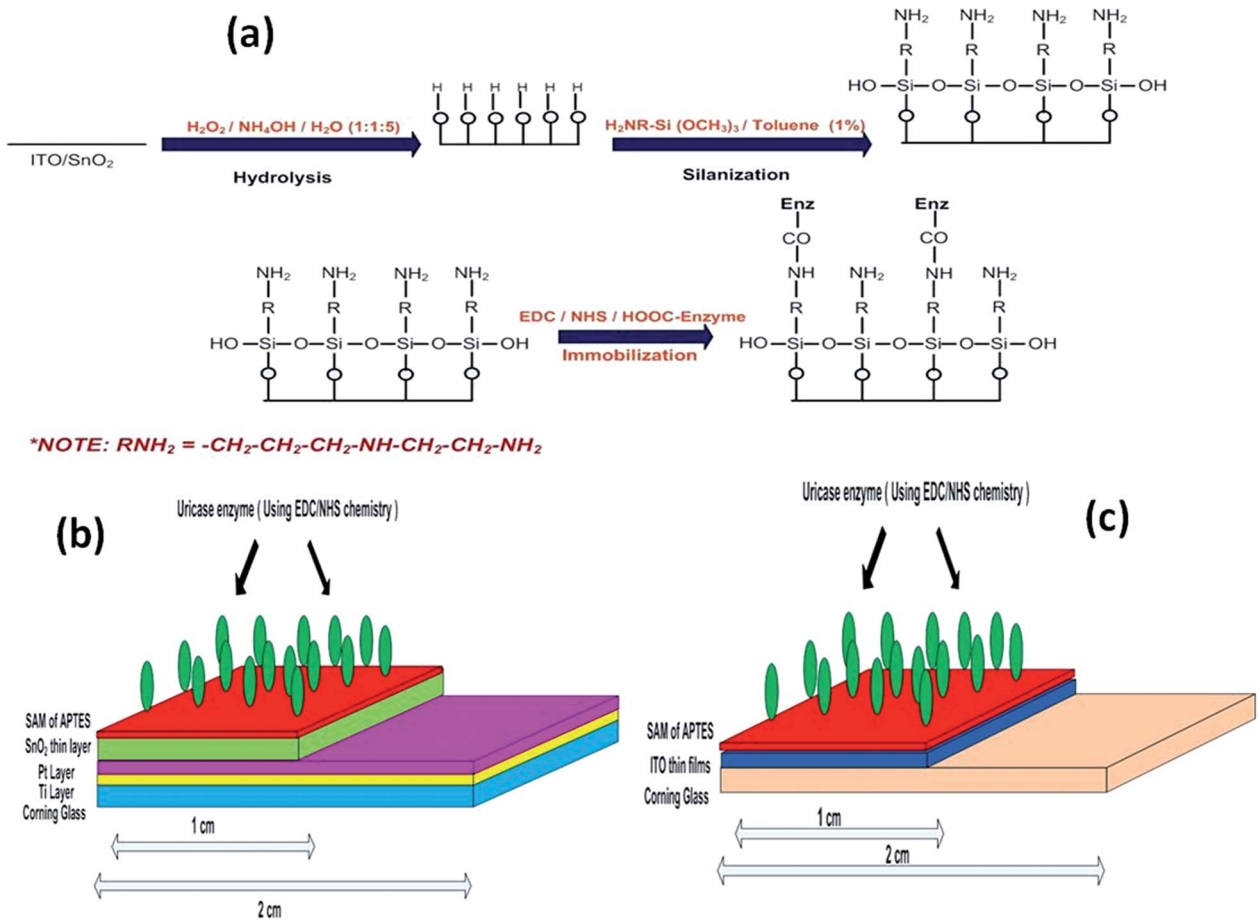

Fig. 1 (a) Schematic showing fabrication of bioelectrodes using EDC/NHS chemistry, (b) schematic of prepared Ur/SnO_2/Pt/Ti/glass, and (c) Ur/ITO/glass bioelectrodes.

structure of the prepared SnO_2 thin film and the immobilization of macromolecules of uricase enzyme onto the prepared SnO_2 thin film matrix. Electrochemical measurements (cyclic voltammetry and impedance spectroscopy for charge transfer resistance) were carried out on a Gamry Reference 600 Potentiostat using a conventional three-electrode cell configuration and using Ag/AgCl as a reference electrode. The apparent enzyme activity of the bio-electrodes was studied using UV-visible spectrophotometer (Perkin Elmer, Lambda 35).

Results and discussion

Structural properties

The as-grown SnO_2 thin films were found to be amorphous, and become polycrsytalline after a post deposition annealing treatment at 300 °C for 3 h in air. The annealed SnO_2 thin films were smooth, transparent and strongly adherent to the substrate. Fig. 2 shows the XRD pattern of post deposition annealed SnO_2 thin films grown under varying content of argon (30% to 80%) in the reactive gas mixture (Ar + O_2). Broad and well defined reflections corresponding to (110), (101), (200) and (211) planes of SnO_2 were observed for all the deposited SnO_2 thin films and are in good agreement to the corresponding values reported in other work.[16] It may be seen from Fig. 2 that the SnO_2 films preferred orientation is along (110) plane when grown under low Ar concentration (≤50%) in reactive gas ambient, while

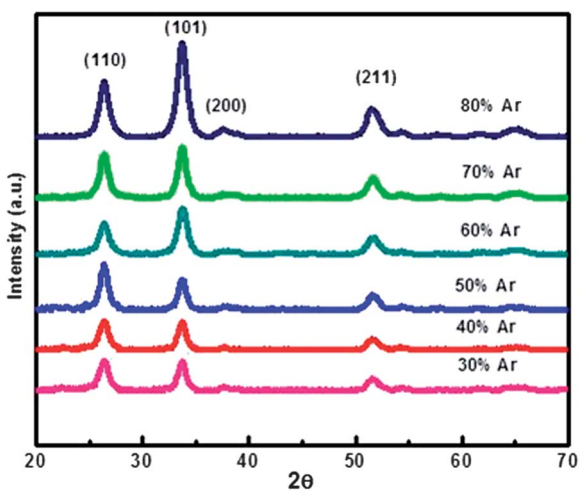

Fig. 2 X-ray diffractogram of the SnO_2 thin films deposited at varying sputtering gas composition (Ar + O_2) and annealed in air at 300 °C for 3 h.

(101) plane becomes dominant for films grown under high Ar percentage (>50%). The values of lattice constants ('*a*' and '*c*') estimated from XRD data for SnO_2 thin films deposited under varying compositions of reactive gas are given in Table 1. The stress modulus along *c*-axis is seen to be decreasing with increasing the O_2% in sputtering gas mixture giving a minimum value (0.094%) for the SnO_2 thin film deposited under 80% Ar and 20% O_2. The well known Scherrer's formula has been used to estimate the crystallite size of deposited SnO_2 thin film using dominant (101) diffraction peak and found to be increasing from 7.9 to 11.4 nm with the increase in the content of oxygen in the reactive sputtering gas from 20% to 70% (Table 1).

Electrical properties

The electrical characteristics of SnO_2 thin films deposited under varying content of argon in the reactive gas mixture (Ar + O_2) from 30% to 80%, including resistivity, carrier concentration and carrier mobility were determined by Hall measurement system using Vander Pauw arrangement. Fig. 3 shows the variation in resistivity, carrier concentration and mobility of charge carriers for SnO_2 thin films with the change in sputtering gas composition. It may be seen from the inset of Fig. 3 that the resistivity of SnO_2 thin films decreases from 912 Ω cm to 4.10 Ω cm with an increase in the percentage of Ar gas in processing reactive gas mixture (≥70%) and saturates thereafter with further increase in Ar content. SnO_2 thin film exhibiting low resistivity, *i.e.*, grown with higher Ar content (≥70%) in reactive gas mixture are expected to yield better charge communication features. However, the carrier concentration is found to increase continuously with increasing Ar percentage in the sputtering gas composition (Fig. 3) which may be attributed to the increase in metallic behaviour of the deposited SnO_2 films. On the contrary, the mobility of charge carriers decreases with an increase in the content of Ar in sputtering gas mixture (Fig. 3). All the SnO_2 thin films deposited with varying concentration of reactive gas were found to exhibit n-type conductivity.

Electrochemical impedance spectroscopy studies

Electrochemical impedance analysis has been performed on a Potentiostat/Galvanostat (Gamry), using a three-electrode cell with the prepared SnO_2 thin films deposited under varying content of argon in the reactive gas mixture (Ar + O_2) from 40% to 80% based electrodes as working electrode, platinum (Pt) foil as counter electrode and Ag/AgCl as reference electrode in PBS solution containing $[K_3Fe(CN)_6]^{3-/4-}$ as the mediator in the frequency range of 100 kHz to 10 mHz. The impedance spectrum (Nyquist plot) includes a semicircle portion corresponding to the electron-transfer-limiting process and a linear part resulting from the diffusion-limiting step of the electrochemical process. The diameter of the semicircle gives the electron-transfer resistance (R_{ct}) of the electrode–solution interface, which controls the electron-transfer kinetics of the redox probe at the electrode interface. Thus, the diameter can be used to describe the interface properties of the electrode. Fig. 4 shows the Nyquist plots obtained for SnO_2 thin film based electrode deposited under varying content of argon in reactive gas mixture. The values of charge transfer resistance (R_{ct}) obtained from Fig. 4 was found to decrease from 912 ohms to 550 ohms with the increase in % of argon from 40% to 70%, which is in accordance with the mobility and carrier concentration of the films as stated above, which implies that conductivity increases with the increase in the percentage of argon in reactive gas mixture.

Optical properties

UV-visible transmission spectra of the SnO_2 thin films deposited under varying gas composition on corning glass slide are shown in Fig. 5. The SnO_2 thin films were found to be highly transparent (~85%) in the visible region (Fig. 5). The optical transmission spectra of all deposited films show a sharp fall at around 307 nm corresponding to the onset of fundamental absorption edge. Band gap of SnO_2 thin films is estimated from the Tauc plot (plot between $(\alpha h\nu)^2$ *versus* $h\nu$, where α is absorption coefficient, and ν is the frequency of incident light). The variation of optical band gap of SnO_2 thin film as a function of Ar content in sputtering gas mixture is shown in the inset of Fig. 5. Bandgap is found to decrease from 3.98 to 3.83 eV (inset of Fig. 5) for SnO_2 films grown with an increase in the content of Ar in reactive gas mixture (Ar + O_2). The observed decrease in bandgap may be attributed to the fact that SnO_2 thin films prepared under low oxygen content in reactive gas are moving towards metallic behaviour. The obtained results are in agreement with the electrical resistivity measurement of SnO_2 thin film (Fig. 3).

Cyclic voltammetric studies

Cyclic voltammetry (CV) studies of the prepared electrodes (SnO_2/Pt/Ti/glass) were carried out on a Gamry Reference 600

Table 1 Variation of XRD parameters with the increasing percentage of Ar in sputtering gas mixture

% of Ar in sputtering gas mixture	XRD peaks at 2θ (°)			$a = b$ (Å)	c (Å)	Crystallite size (nm)	Stress modulus (σ) %
	(110)	(101)	(211)				
30	26.40	33.90	51.51	4.787	3.178	11.4	0.251
40	26.41	33.84	51.59	4.777	3.179	10.9	0.219
50	26.42	33.80	51.62	4.767	3.191	10.6	0.156
60	26.43	33.79	51.62	4.763	3.191	10	0.156
70	26.50	33.76	51.65	4.774	3.191	9	0.156
80	26.52	33.76	51.65	4.766	3.189	7.9	0.094
Bulk SnO_2	26.61	33.89	51.78	4.737	3.186	—	—

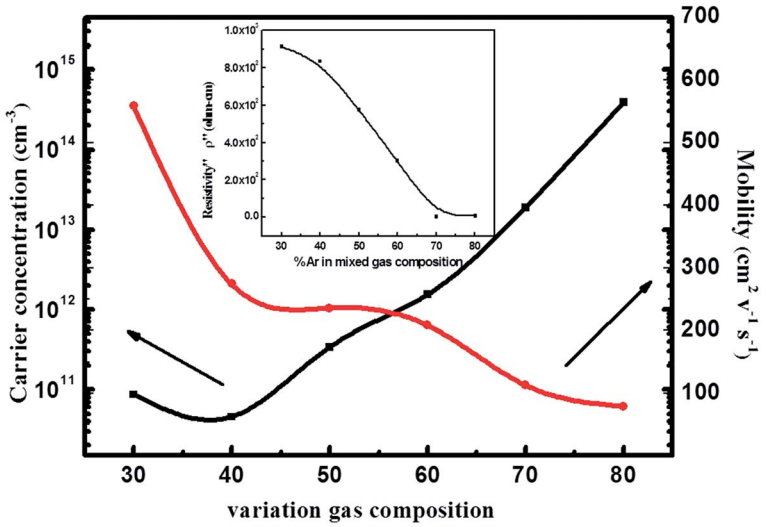

Fig. 3 Variation of carrier concentration and mobility as a function of percentage of Ar in sputtering gas mixture (Ar + O_2). Inset shows the variation in electrical resistivity of SnO_2 thin film with composition of processing reactive gas.

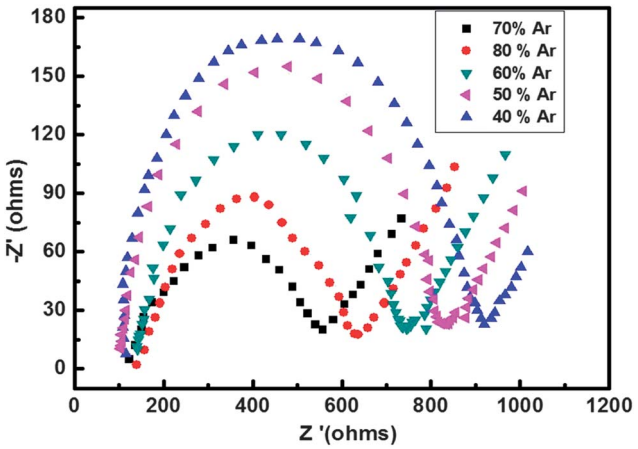

Fig. 4 Electrochemical impedance spectroscopy (EIS) of prepared SnO_2 thin film based matrix deposited under varying % of argon in reactive gas mixture.

Potentiostat/Galvanostat using a three-electrode cell configuration with Ag/AgCl as a reference electrode and the platinum foil as a counter electrode in 10 ml of phosphate buffer saline (PBS) solution (50 mM, pH 7.0, 0.9% NaCl) containing a mixture of 5 mM $Fe(CN)_6^{4-}$ (ferrocyanide) and 5 mM of $Fe(CN)_6^{3-}$ (ferricyanide), *i.e.*, 5 mM $Fe(CN)_6^{3-/4-}$ as a redox probe. Using the redox probe (5 mM $Fe(CN)_6^{3-/4-}$) charge transfer process at electrode–electrolyte interface has been investigated.

Fig. 6 shows the cyclic voltammograms measured as a function of applied bias in the range from −0.3 V to 0.8 V for the prepared electrodes (SnO_2/Pt/Ti/glass) having SnO_2 matrix deposited under varying content of argon in the reactive gas mixture (Ar + O_2) from 30% to 80%. It is important to point out that for SnO_2 thin films deposited under lower Ar percentage (≤50%) in the sputtering gas composition, no significant redox peaks are visible (Fig. 6). However, well defined oxidation and reduction peaks are observed in the CV spectra of electrodes having SnO_2 films grown under higher Ar content (>50%) in the sputtering gas composition. The values of peak oxidation (I_{pa}) and reduction (I_{pc}) currents obtained for all prepared electrodes are summarized in a table given in the inset of Fig. 6.

The appearance of redox peak in CV spectra of electrodes may be attributed to the electron communication property of SnO_2 thin film matrix while in turn it depends on its electrical conductivity and presence of native defects. The SnO_2 thin film with preferred orientation along the (101) plane as observed in the films grown under higher Ar content (>50%) in reactive ambient is generally related with the non stoichiometric phase having native defects related to oxygen vacancies, thereby the concentration of free electrons in conduction band of SnO_2 is relatively higher.[17] On the other side the dominating XRD peak along the (110) plane (when films are grown under low Ar content (≤50%) in reactive gas) is attributed to the stoichiometric phase having relatively lower concentration of free electrons.[18] Hence the SnO_2 thin film matrix grown under low Ar content (≤50%) exhibits high resistivity (Fig. 3) and does not show any redox peak in the CV spectra (Fig. 6).

Peak oxidation current (I_{pa}) is found to be increasing for SnO_2 matrix grown with decreasing oxygen content in reactive gas ambient from 40% to 30%, and is due to a decrease in resistivity of film (Fig. 4). However, for SnO_2 film grown with further decreasing the oxygen percentage in reactive gas mixture to 20%, peak oxidation current was almost found to saturate. SnO_2 thin film (grown under 70% Ar and 30% O_2) which exhibits well defined oxidation and reduction peaks along with high value of I_{pa} obtained in the CV spectra was chosen for further biosensing studies.

The uricase was immobilized on the surface of SnO_2/Pt/Ti/glass and ITO/glass electrodes using covalent bonding as explained earlier. The immobilization of enzyme on the surface of these electrodes is studied using FTIR and AFM studies, as discussed below.

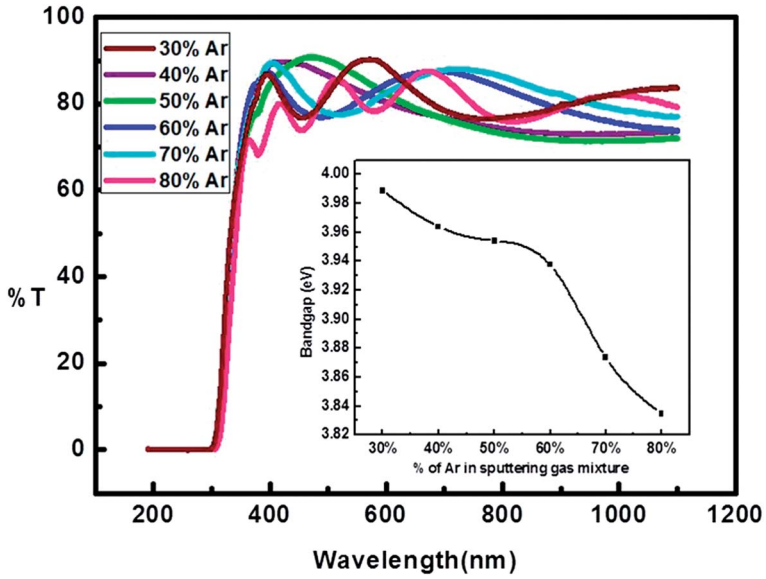

Fig. 5 Influence of variation of Ar on the transmission spectra of SnO_2 thin film.

FTIR spectroscopy

The FTIR spectra of SnO_2/Pt/Ti/glass electrodes is also included in Fig. 7(i). The FTIR spectra of uricase/SnO_2/Pt/Ti/glass and uricase/ITO/glass bioelectrodes are shown in Fig. 7(ii) for comparison. The absorption band observed at around 606 cm^{-1} corresponds to the SnO_2 lattice mode,[20] confirming the formation of SnO_2 thin film [Fig. 7(i)]. The absorption band observed at around 3356 cm^{-1} can be assigned to the surface –OH groups attached directly to the oxygen of the SnO_{2-x},[19] and the absorption band at 1633 cm^{-1} is attributed to H–O–H in plane deformation. The modes at 2154, 2373 and 2924 cm^{-1} correspond to O–H stretching, stretching vibrations of hydroxyl group and ν(CH) vibrations, respectively. The appearance of additional bands at around 1568 and 1650 cm^{-1} [Fig. 7(ii)] correspond to the primary and secondary amide linkages of enzyme molecules (uricase) indicating the immobilization of uricase on the surfaces of SnO_2 and ITO thin film.[21] The additional absorption bands at 990, 1085 and 1708 cm^{-1} [Fig. 7(ii)] correspond to C–H bending of alkene, C–N vibrations and C═O stretching mode, respectively. The bands at 2922 and 3462 cm^{-1} correspond to C–H stretching vibrations and O–H stretching, respectively [Fig. 7(ii)].[22] The observed results clearly confirm the successful immobilization of enzyme (uricase) on the surface of the SnO_2 and ITO based electrodes.

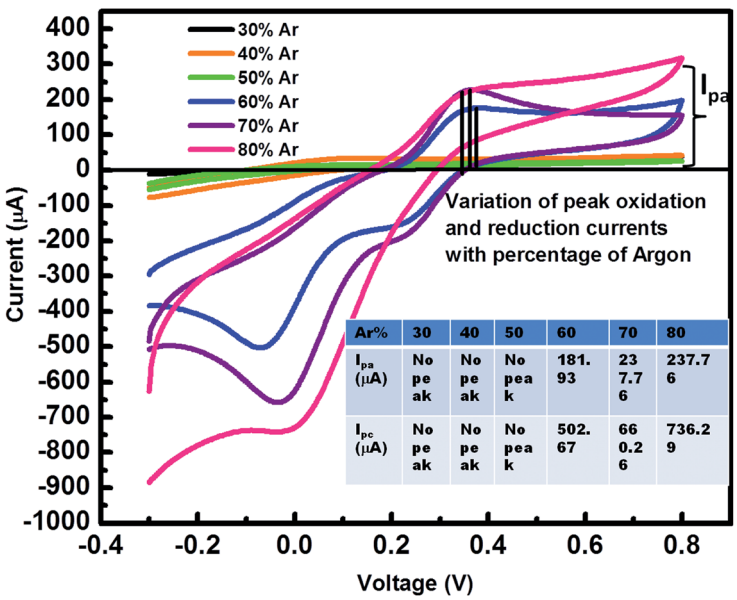

Fig. 6 CV response of the SnO_2 thin film electrodes deposited under varying Ar percentage in the sputtering gas mixture.

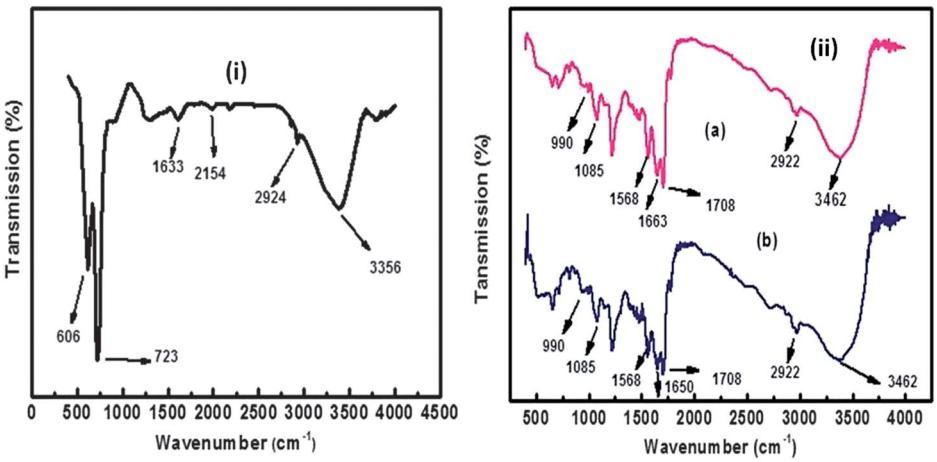

Fig. 7 (i) FTIR spectra of SnO_2/Pt/Ti/glass electrode, (ii) FTIR spectra of Ur/SnO_2/Pt/Ti/glass and Ur/ITO/glass bioelectrodes showing efficient immobilization of uricase on the surface of respective electrodes.

Atomic force microscopy (AFM)

Fig. 8(a) shows the AFM image of the surface of SnO_2 thin film deposited at optimized growth conditions (14 mTorr and reactive ambient of 70% Ar + 30% O_2). The rough surface morphology having nanopores microstructure of SnO_2 thin film [Fig. 8(a)] provides larger surface area which is advantageous for enhanced enzyme loading. Fig. 8(b) shows the AFM image of the commercially procured ITO coated glass substrate. The surface microstructure of ITO film was found to be fine having uniformly distributed grains along with nanoporous morphology. It may be easily seen from Fig. 8(a) and (b) that the grain size and surface roughness of SnO_2 thin film is much more compared to that observed for ITO film. AFM micrograph of the surface of uricase/SnO_2/Pt/Ti/glass and uricase/ITO/glass bioelectrodes shows an aggregation of globular shaped cross linked enzyme molecules [Fig. 8(c) and (d)]. SnO_2 thin films having high surface roughness and grain size, yield in the immobilization of biomolecules large size globular structure in comparison to that on ITO surface.

Scanning electron microscopy (SEM) studies

The surface morphologies of (i) SnO_2/Pt/Ti/glass electrode and (ii) uricase SnO_2/Pt/Ti/glass bioelectrode have been studied

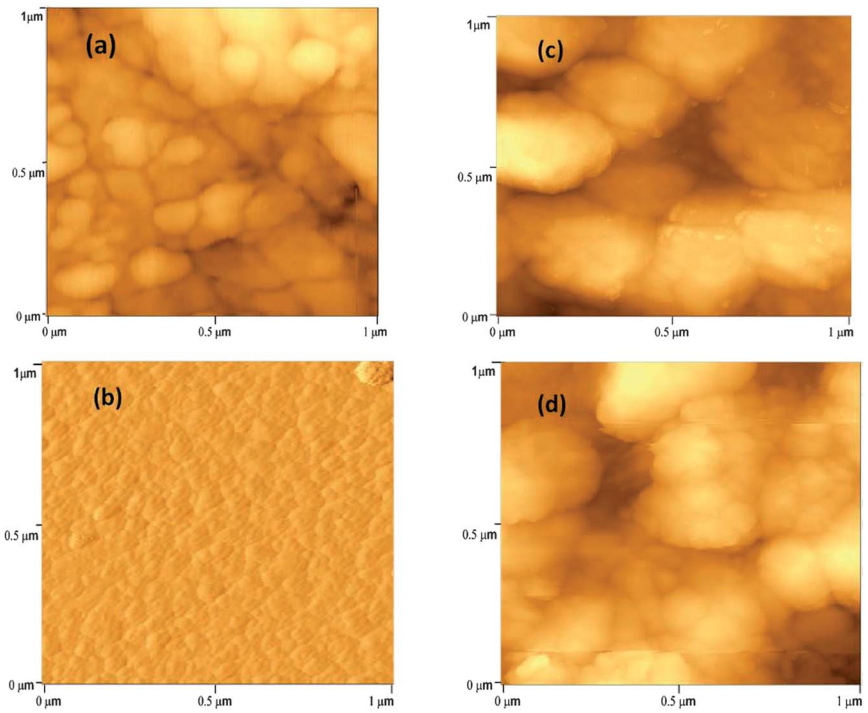

Fig. 8 AFM image of the surface of (a) SnO_2/Pt/Ti/glass electrode, (b) ITO/glass electrode, (c) Ur/SnO_2/Pt/Ti/glass bioelectrode and (d) Ur/ITO/glass bioelectrode.

using SEM and images are shown in Fig. 9(i) and (ii), respectively. The surface of SnO_2 thin film shows a fine homogeneous morphology having uniformly distributed nanosize crystallites [Fig. 9(i)]. The surface morphology becomes rough after immobilization of macro molecules of uricase enzyme (~2 μm) onto the surface of SnO_2/Pt/Ti/glass electrode. The uniformly distributed globular structures observed in the SEM image of the surface of uricase/SnO_2/Pt/Ti/glass bioelectrode [Fig. 9(ii)] reveals successful immobilization of uricase enzyme with homogeneous coverage and dense loading.

Amperrometric response characteristics

Fig. 10 shows the cyclic votammograms recorded in the range of −0.3 to 0.8 V for the SnO_2/Pt/Ti/glass electrode (i) before and (ii) after enzyme immobilization. The peak oxidation current (I_{pa}) for the SnO_2/Pt/Ti/glass electrode is found to be decreasing from 267 μA to 140 μA on immobilization of uricase (uricase/SnO_2/Pt/Ti/glass) and is attributed to the non conducting nature of macromolecular enzymes which hinder the flow of charge carriers from the electrolyte to the electrode.

The cyclic voltammograms of (i) ITO/glass electrode and (ii) uricase/ITO/glass bioelectrode obtained in PBS solution are shown in Fig. 11. As discussed earlier, due to the non conducting nature of the macromolecules of uricase enzyme a decrease in the peak oxidation current is observed from 355 μA to 266 μA on enzyme immobilization on the surface of ITO/glass electrode. The obtained results signify that both the electrodes (based on SnO_2 and ITO matrix) provide a three-dimensional biocompatible environment to the enzyme (uricase) molecules and hence confirms the immobilization of uricase on their surface. Furthermore it may be noted from Fig. 10 and 11 that the value of peak oxidation current obtained for ITO/glass electrode (355 μA) is much higher as compared to the corresponding value (267 μA) obtained for the prepared SnO_2/Pt/Ti/glass electrode and is attributed to the high conductivity of ITO film.

The concentration of ionic species on the surfaces of uricase/SnO_2/Pt/Ti/glass and uricase/ITO/glass bioelectrodes is estimated from the CV studies as a function of scan rate (ν) from 100 to 180 mV s^{-1} and the variations are shown in Fig. 12 and 13, respectively. For both the bioelectrodes, the oxidation peak is found to shift slowly towards higher potential and the reduction peak towards the lower potential, with an increase in scan-rate from 100 to 180 mV s^{-1} (Fig. 12 and 13) indicating that the involved process is a

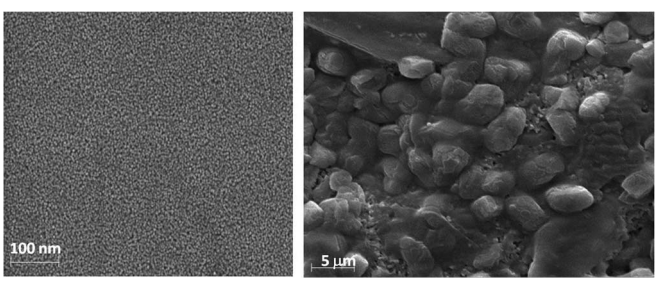

Fig. 9 Scanning electron microscopy (SEM) images of SnO_2 and uricase immobilized on SnO_2 thin film based matrices.

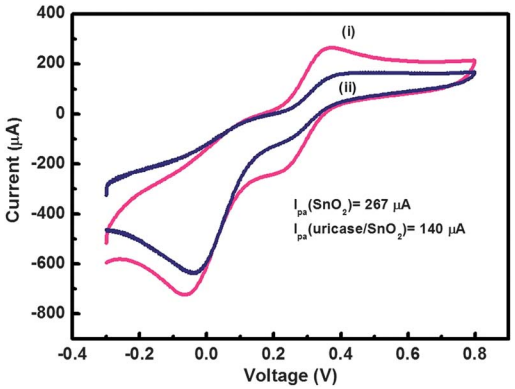

Fig. 10 Cyclic voltammogram of (i) SnO_2/Pt/Ti/glass electrode and (ii) Ur/SnO_2/Pt/Ti/glass bioelectrode.

quasi-reversible process. The values of both the anodic (I_{pa}) and cathodic (I_{pc}) peak currents increase linearly with the square root of scan rate ($\nu^{1/2}$) (insets in Fig. 12 and 13) for both the bioelectrodes (uricase/SnO_2/Pt/Ti/glass and uricase/ITO/glass), suggesting that the electrode reaction is a diffusion assisted electron-transfer process. Furthermore, the potential corresponding to oxidation peak and reduction peak was found to vary directly with sweep rate, indicating improved electrocatalytic behavior.

The linear regression equations for the peak oxidation (I_{pa}) and peak reduction (I_{pc}) currents are given as:

For Ur/SnO_2/Pt/Ti/glass bioelectrode:

$$I_{pa} = 20.54(\nu)^{1/2} - 102.28 \text{ with, } R = 0.99; \quad (1)$$

$$I_{pc} = -66.67(\nu)^{1/2} + 232.66 \text{ with, } R = 0.99; \quad (2)$$

For Ur/ITO/glass bioelectrode:

$$I_{pa} = 48.93(\nu)^{1/2} - 373.29 \text{ with, } R = 0.99; \quad (3)$$

$$I_{pc} = -42.22(\nu)^{1/2} + 292.99 \text{ with, } R = 0.99; \quad (4)$$

where R is regression coefficient. The anodic peak potential (E_{pa}) also varies linearly with logarithm of ν and follows the equation:

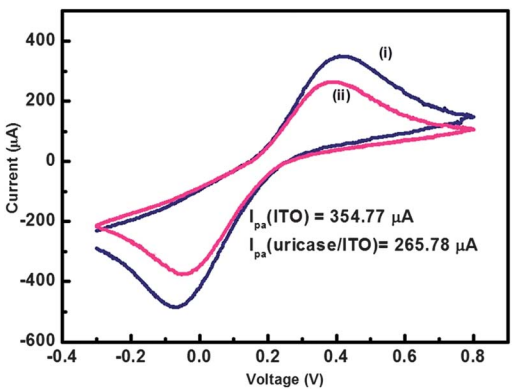

Fig. 11 Cyclic voltammogram of (i) ITO/glass electrode and (ii) Ur/ITO/glass bioelectrode.

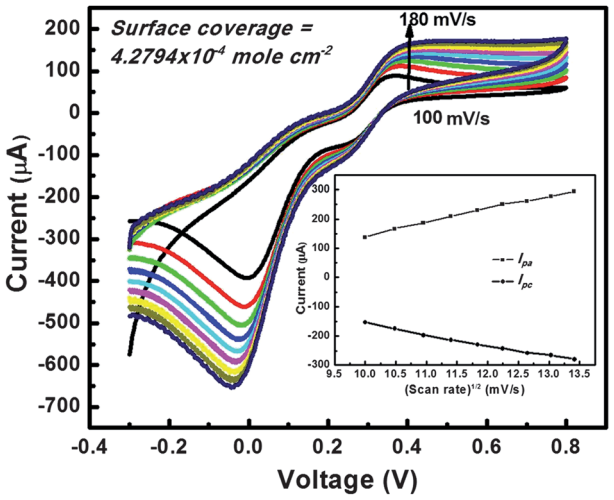

Fig. 12 CV spectra of Ur/SnO_2/Pt/Ti/glass bioelectrode with varying scan rate from 100 to 180 mV s^{-1}; inset: magnitudes of peak oxidation (I_{pa}) and reduction (I_{pc}) currents as a function of (scan rate)$^{1/2}$.

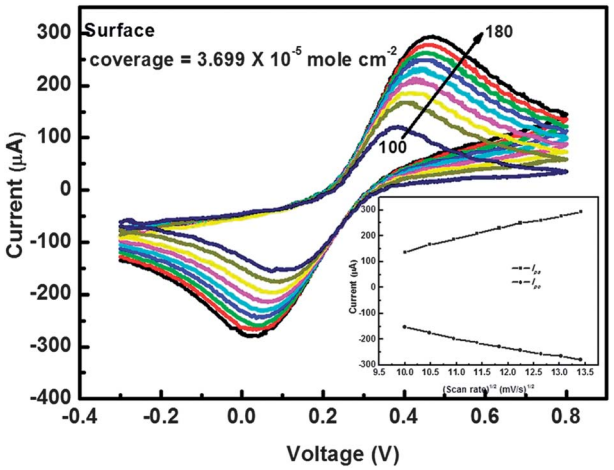

Fig. 13 CV spectra of Ur/ITO/glass bioelectrode with varying scan rate from 100 to 180 mV s^{-1}; inset: magnitudes of peak oxidation (I_{pa}) and reduction (I_{pc}) currents as a function of (scan rate)$^{1/2}$.

(Ur/SnO_2/Pt/Ti/glass bioelectrode)

$$E_{pa} = 0.3483 \log \nu - 0.3263 \text{ with, } R = 0.99; \quad (5)$$

(Ur/ITO/glass bioelectrode)

$$E_{pa} = 0.2874 \log \nu - 0.2195 \text{ with, } R = 0.99; \quad (6)$$

The value of regression coefficient close to 1.0 in all the eqn (1)–(6) suggests that the variation of I_{pa}, I_{pc} and E_{pa} follows a perfect linear fit for both the bioelectrodes (Ur/SnO_2/Pt/Ti/glass and Ur/ITO/glass). According to Laviron's theory, slope of the plot between E_{pa} *versus* log ν, *i.e.*, $RT/\alpha nF$ is about 0.29 and 0.35, respectively, for Ur/SnO_2/Pt/Ti/glass and Ur/ITO/glass bioelectrodes, where, R is the gas constant (8.314 J mol^{-1} K^{-1}), F is the Faraday constant (96 485 C mol^{-1}), T is the operating temperature (300 K), n is the number of electrons transferred (1) and α is the transfer coefficient. The value of slope can further be used to estimate the total surface concentration of the ionic species (I^*). The surface concentration (I^*) of the ionic species on the surface of uricase/SnO_2/Pt/Ti/glass and uricase/ITO/glass bioelectrodes is estimated using the Brown–Anson model based on the following equation:[23]

$$I_{pa} = \frac{n^2F^2I^*A\nu}{4RT} \quad (7)$$

where I^* is the estimated value of surface coverage of bioelectrodes in mol cm^{-2}; I_{pa}/ν can be calculated from the slope of I_{pa} *vs.* ν plot. The surface coverage of uricase/SnO_2/Pt/Ti/glass and uricase/ITO/glass bioelectrodes were found to be about 4.28×10^{-4} and 3.7×10^{-5} mol cm^{-2}, respectively, which are much higher in comparison to the corresponding values reported in literature for other inorganic matrices based bioelectrodes for uric acid,[24] and indicates the better immobilization of enzyme in the present work. Furthermore, SnO_2 based bioelectrode shows one order higher surface coverage compared to ITO based bioelectrode. The higher surface coverage obtained for SnO_2 matrix is attributed to comparatively high porosity and large surface roughness of deposited SnO_2 thin film [Fig. 8(a) and (b)] which is providing favourable surface for enzyme to be immobilized.

The biosensing activities of Ur/SnO_2/Pt/Ti/glass and Ur/ITO/glass bioelectrodes were investigated by CV measurements in a mediated PBS solution having different concentrations of uric acid, and are shown in Fig. 14 and 15, respectively. The oxidation peak current for both Ur/SnO_2/Pt/Ti/glass and Ur/ITO/glass bioelectrodes was found to increase linearly with an increase in uric acid concentration from 0.05 mM to 1 mM (0.84 mg dl^{-1} to 16.8 mg dl^{-1}) (Fig. 14 and 15). Uricase catalyzes the *in vivo* oxidation of uric acid in the presence of oxygen to produce allantoin and CO_2 as oxidation products of uric acid, and hydrogen peroxide as a reduction product of O_2.

The uricase catalytic reaction is as follows:

$$\text{Uric acid} + H_2O + O_2 \xrightarrow{\text{uricase}} \text{allantoin} + CO_2 + H_2O_2 \quad (8)$$

Formation of hydrogen peroxide is detected by the amperometric current method during oxidation at the electrode which takes place at a relatively high potential (>0.5 V):

$$H_2O_2 \rightarrow O_2 + 2H^+ + 2e^- \quad (9)$$

The enzymatic electrochemical biosensor relies on shuttling of these electrons, generated in the biochemical reaction (eqn (9)), from the redox center of the enzyme (uricase) to the electrode *via* SnO_2 or ITO thin film matrix. The redox centers of enzymes, because of their insulated-shell, are unable to show direct electrochemistry. The presence of external redox species (mediator $[Fe(CN)_6]^{3-/4-}$), in the PBS system, provides the path for electron transfer at a much lower potential (<0.5 V) from the redox centers of the enzyme to the electrode using a good electron communication property of the metal oxide matrix, which results in increase in the peak oxidation and reduction currents. No peak corresponding to the oxidation of H_2O_2 is

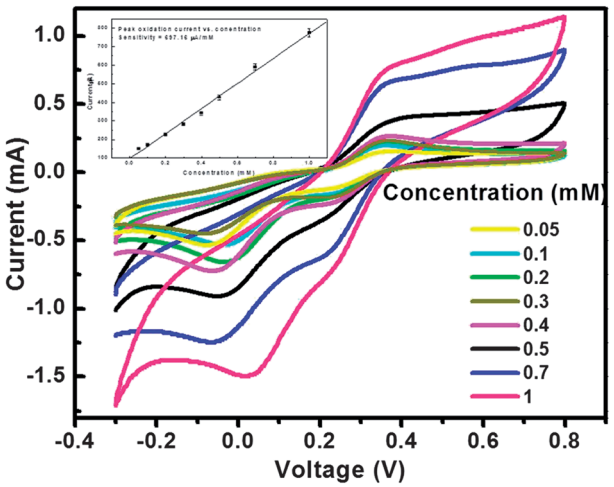

Fig. 14 Electrochemical sensing response of Ur/SnO_2/Pt/Ti/glass bioelectrode with increase in uric acid concentration; inset: variation of peak oxidation current as a function of uric acid concentration.

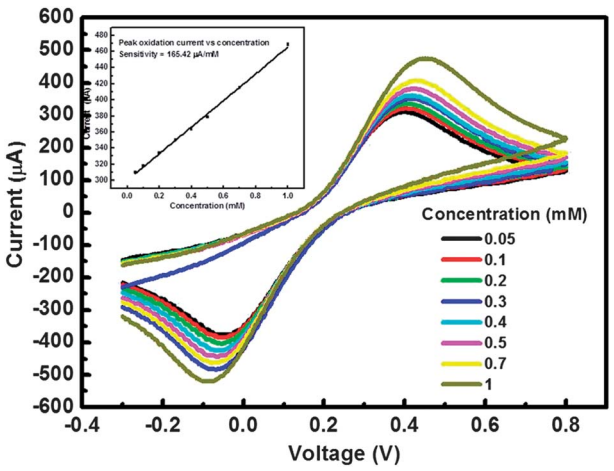

Fig. 15 Electrochemical sensing response of Ur/ITO/glass bioelectrode with increase in uric acid concentration; inset: variation of peak oxidation current as a function of uric acid concentration.

noted in the working potential window of the CVs of the prepared bio-electrodes (Fig. 14 and 15). The presence of $K_3[Fe(CN)_6]$ in the PBS solution acts as an efficient electron acceptor over bio-oxygen, resulting in an oxidation peak at a potential of about 0.36 V and 0.47 V, respectively, for Ur/SnO_2/Pt/Ti/glass and Ur/ITO/glass bioelectrodes (Fig. 14 and 15).

The continuous rise in the peak oxidation current from 151 μA to 774 μA and 307 μA to 477 μA for Ur/SnO_2/Pt/Ti/glass and Ur/ITO/glass bioelectrodes, respectively, with increasing concentration of uric acid from 0.05 to 1.0 mM (insets of Fig. 14 and 15) is attributed to the release of more electrons in the catalytic oxidation of uric acid by uricase. It is clear from the insets of Fig. 14 and 15 that Ur/SnO_2/Pt/Ti/glass and Ur/ITO/glass bioelectrodes show good linearity over a wide range of uric acid concentrations from 0.05–1.0 mM with lower detection limit of about 0.04 mM and 0.046 mM respectively. The experiments were carried out in triplicate sets, and results were found to be reproducible within 5% as shown by the error bars in the Fig. 14 and 15. The values of different sensing parameters obtained for the Ur/SnO_2/Pt/Ti/glass and Ur/ITO/glass bioelectrodes are summarized in Table 2. It is important to point out that Ur/ITO/glass bioelectrode exhibits the high value of initial current (307 μA) in comparison to the corresponding value of 151 μA obtained for Ur/SnO_2/Pt/Ti/glass bioelectrode. However, the Ur/SnO_2/Pt/Ti/glass bioelectrode provides a much higher change in peak oxidation current for the same concentration of the analyte (uric acid), and is attributed to the better electron communication feature of the prepared SnO_2 thin film compared to that of ITO. The sensitivity calculated from the plot of linear variation of peak oxidation current *versus* uric acid concentration was found to be about 697 μA mM^{-1} and 165 μA mM^{-1} for Ur/SnO_2/Pt/Ti/glass and Ur/ITO/glass bioelectrodes, respectively. The high value of initial current (I_{pa}) obtained for ITO based bioelectrode may be because of the low resistivity (0.23 Ω cm) offered by ITO film compared to SnO_2 thin film. On the other side, the high value of carrier mobility of SnO_2 thin film (113 $cm^2 V^{-1} s^{-1}$) may be responsible for the large variation in peak oxidation current on interaction with uric acid and hence results in enhanced sensitivity. The response time of both the bioelectrodes is about 5 s which is fast compared to the corresponding reported values. The biosensing response characteristics (sensitivity, detection limit, surface coverage of enzyme, linear range) obtained for the bioelectrodes based on SnO_2 and ITO matrices in the present case are found to be superior than those reported in literature by various workers on other metal oxide matrices (Table 3).

Estimation of Michaelis–Menten kinetic parameters K_m^{app}

The Michaelis–Menten kinetic parameter (K_m^{app}) of enzymatic reaction has been estimated using Hanes plot (*i.e.*, graph between [analyte concentration] and [analyte concentration/current]) shown in Fig. 16 for both the Ur/SnO_2/Pt/Ti/glass and Ur/ITO/glass bioelectrodes. The Hanes plot for both the bioelectrodes are found to be straight lines and the value of K_m^{app} is estimated to be 0.18 mM and 0.48 mM for the uricase immobilized on the surface of SnO_2/Pt/Ti/glass and ITO/glass electrodes, respectively. The obtained values of K_m^{app} are also summarized in Table 2. The much lower value of K_m^{app} for SnO_2 based electrode in the present work that SnO_2 acts as a better matrix for enzyme loading and the lower value of K_m^{app} (~0.18 mM) is reflecting the enhanced activity of immobilized uricase on the surface of SnO_2 matrix towards the analyte (uric acid). The increased interaction between the enzyme's active sites and the analyte is due to the favorable conformational changes in the enzyme structure on being immobilized on the nanoporous and rough surface of SnO_2 thin film matrix and are facilitated by the suitable biocompatible microenvironment provided by the SnO_2 thin film in comparison to ITO film.

Photometric enzyme assay

UV-visible spectrophotometer has been used to study the activity of Ur/SnO_2/Pt/Ti/glass and Ur/ITO/glass bioelectrodes

Table 2 Comparison between experimentally observed various properties of two prepared bioelectrodes

Properties	Tin oxide as a matrix (at optimized growth parameter)	ITO as a matrix (procured commercially)
Resistivity (Ω cm)	4.10	0.23
Carrier concentration (cm^{-3})	1.88×10^{13}	1.33×10^{18}
Mobility ($cm^2\ v^{-1}\ s^{-1}$)	113	59
Band gap (eV)	3.85	3.78
Linearity (mM)	0.05–1.00	0.05–1.00
Sensitivity ($\mu A\ mM^{-1}$)	698	165
Surface coverage of enzyme (mole cm^{-2})	4.28×10^{-4}	3.70×10^{-5}
Michaelis–Menten constant (K_m) (mM)	0.18	0.48
Enzyme activity (units cm^{-2})	4.41×10^{-2}	1.85×10^{-2}
Detection limit (mM)	0.04	0.046

using photometric enzymatic assay. The bioelectrodes were dipped in 3 ml PBS solution containing 20 μl HRP, 20 μl *o*-dianisidine dye, and 100 μl analyte (uric acid) for approximately 2 minutes. The difference between the values of initial and final absorbance at $\lambda = 500$ nm after the 2 min incubation of uric acid in different concentrations was recorded and plotted in Fig. 17 for both the bioelectrodes. In the reaction mixture, the following biochemical reaction occurs:

$$[\text{ITO/glass or } SnO_2\text{/Pt/Ti/glass} - \text{uricase}_{oxi}] + \text{uric acid} + O_2 \rightarrow [\text{ITO/glass or } SnO_2\text{/Pt/Ti/glass} - \text{uricase}_{red}] + \text{allantoin} + H_2O_2 \quad (10)$$

$$H_2O_2 + o\text{-dianisidine}_{(reduced)} \xrightarrow{HRP} 2H_2O + o\text{-dianisidine}_{(oxidised)}[\text{orange red colour}] \quad (11)$$

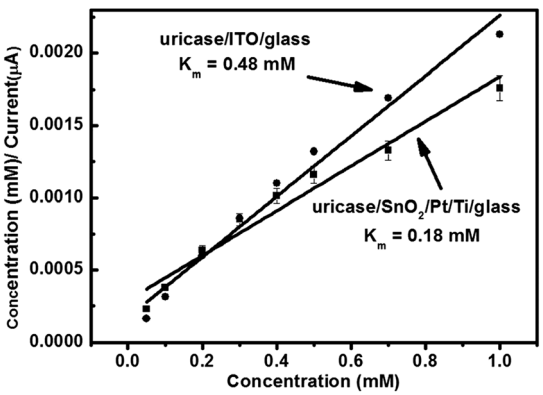

Fig. 16 Hanes plot between the analyte concentration and analyte concentration/current for Ur/SnO_2/Pt/Ti/glass and Ur/ITO/glass bioelectrodes.

Table 3 Work done on uric acid biosensors by different workers using various matrices

S. No.	Material	Range	Sensitivity	Response time	Km	Detection limit	*S*/*N*	Reference
1.	SAM of APTES bis sulfosuccinimide/ITO	0.05–0.58 mM	39.35 $\mu A\ mM^{-1}$	50 s		0.037 mM	3	12
2.	Polypyrrole/Pt	7.5×10^{-11} –8.3×10^{-6} M			3.4×10^{-7} M	75 pM	—	31
3.	Ir–C electrode	0.1–0.8 mM	16.60 $\mu M\ mM^{-1}$	<45 s		0.01 mM	6.18	32
34.	SAM thio-substituted nucleobases/Au	1–500 μM	0.78 $\mu A\ \mu M^{-1}\ cm^{-2}$	8 s		1 μM	—	25
5.	Mercaptoethylpyrazine/Au	5–150 μM	3.4 ± 0.08 nA cm−2 μM^{-1}	80–100 s	290 μM	2 μM	3	26
6.	Polystyrene sulfonate/ MWCNTs/graphite	1–6 mM	291 $\mu A\ mM^{-1}$			8.0×10^{-7} M	—	33
7.	MWCNT-Ch/ poly(amidoamine)/ DNA/gold electrode	0.5–100 μM	43.9 $nA\ mM^{-1}$	5 s		0.07 μM	3	34
8.	Polyaniline	0.01–0.6 mM	47.2 $mA\ mM^{-1}$	60 s	5.1×10^{-3} mM L^{-1}	0.01 mM	—	35
9.	Carbon ceramic electrode	1–50 μM and 0.5–20 μM	0.0303 $\mu A\ \mu M^{-1}$ and 0.754 $\mu A\ \mu M^{-1}$			0.4 μM and 0.1 μM	3	36
10.	MWCNTS/PMAA	80–500 μM	11.03 and 5.39 mA $M^{-1}\ cm^{-2}$	5 min		22 μM	>3	37
11.	Hb encapsulate chitosan modified GCE	2–30 μM	29.5 $\mu A\ mM^{-1}$	60 s		0.85 μM	3	38
	SnO_2/Pt/Ti/glass and ITO/ glass electrodes	0.05–1 mM	697.16 $\mu A\ mM^{-1}$ and 165.42 $\mu A\ mM^{-1}$	5 s	0.18 mM and 0.48 mM	0.04 mM and 0.048 mM	3	Present work

Absorption rate is related to the concentration of H_2O_2 produced in the reaction, which is directly proportional to uric acid concentration. Using the above reaction system, we can calculate the activity of the reaction. The enzyme activity increases with increasing uric acid concentration initially, and thereafter saturates for about concentration >0.7 mM for both the bioelectrodes. The amount of bound enzyme is determined from the apparent enzyme activity (a_{enz}^{app}) calculated using:

$$a_{enz}^{app}(\text{U cm}^{-2}) = \frac{AV}{\varepsilon ts} \quad (12)$$

where A is the difference in the values of absorbance before and after incubation, V is the total volume (= 3.17 cm^3), ε is the millimolar extinction coefficient for *o*-dianisidine (7.5 for *o*-dianisidine at 500 nm), t is the reaction time (2 min), and s is the surface area of the bioelectrode. The values of apparent enzyme activity (U cm^{-2}) of the immobilized uricase on the surface of SnO_2/Pt/Ti/glass and ITO/glass electrodes were found to be about 4.41×10^{-2} unit per cm^2 and 1.85×10^{-2} unit per cm^2, respectively (Table 2), indicating that more units of uricase are actively working on unit surface area of bioelectrode in case of SnO_2 matrix as compared to the ITO matrix. This may be related to the porous and rough surface morphology of the prepared SnO_2 thin film which provides a suitable platform for the immobilization of enzyme (uricase) and subsequently their activity.[27] No report is available in literature on the enzyme activity of uricase immobilized on the surface of SnO_2 matrix. However, the activity of immobilized uricase for SnO_2 matrix in the present work is much better as compared to that obtained by other workers on various matrices.[28,29]

Interference and shelf life

The selectivity of Ur/SnO_2/Pt/Ti/glass and Ur/ITO/glass bioelectrodes are determined by measuring response current in CV analysis on addition of normal concentration of different interferents present in the human serum such as glucose (5.6 mM), cholesterol (5 mM), ascorbic acid (0.1 mM), lactic acid (0.5 mM) and urea (1 mM) to the normal concentration of uric acid (0.1 mM). A maximum interference of about 2% was obtained using both the bioelectrodes. The shelf life studies of the prepared Ur/SnO_2/Pt/Ti/glass and Ur/ITO/glass bioelectrodes shows that both bioelectrodes retain more than 90% of their activity even after 4 months which is much higher compared to the corresponding reports available on other biosensors based on metal oxides[30] and also 30 times reusable with maintained activity.

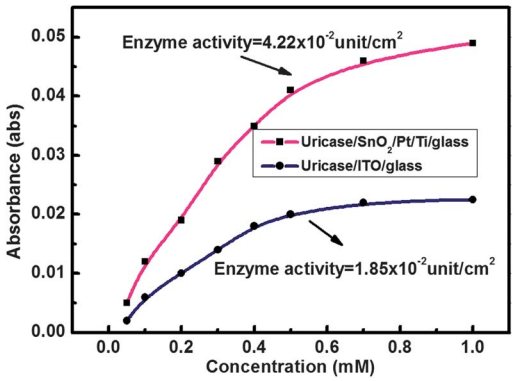

Fig. 17 Photometric study of the prepared bioelectrodes (Ur/SnO_2/Pt/Ti/glass and Ur/ITO/glass) with uric acid concentration.

Conclusions

SnO_2 thin film deposited under 70% Ar and 30% O_2 in the sputtering gas environment has been identified as a promising matrix exhibiting optimum electrical and structural properties for biosensing applications. The sensing response characteristics for uric acid on SnO_2 matrix are compared with those obtained on ITO matrix. Uricase is covalently immobilized onto two-dimensional SAM of APTES using EDC/NHS chemistry for the realization of bioelectrodes (Ur/SnO_2/Pt/Ti/glass and Ur/ITO/glass). The enhanced sensitivity of Ur/SnO_2/Pt/Ti/glass bioelectrode (697 μA mM^{-1}) is attributed to the high mobility of the prepared SnO_2 thin film matrix. A linear range of detection of uric acid from 0.05 mM to 1 mM with a low detection limit of 0.04 mM was obtained. The low value of Michaelis–Menten constant (0.18 mM) for Ur/SnO_2/Pt/Ti/glass bioelectrode confirms that the SnO_2 matrix provides an efficient platform for immobilization of uricase, where the enzyme not only retains its bioactivity but maintains a confirmation thereby giving enhanced enzyme activity. The apparent enzyme activity for Ur/SnO_2/Pt/Ti/glass bioelectrode (4.41×10^{-2} unit per cm^2) was much higher in comparison to that obtained for Ur/ITO/glass bioelectrode (1.85×10^{-2} unit per cm^2), indicating a biocompatible environment provided by SnO_2 matrix for efficient immobilization of enzyme. The prepared bioelectrode exhibits a long shelf life of more than 4 months and much higher reusability (30 times).

Acknowledgements

Authors are thankful to the Department of Science and Technology (DST) and UGC for the financial support to carry out the proposed work. One of the authors (KA) acknowledges CSIR for fellowship.

References

1 J. Galban, Y. Andreu, M. J. Almenara, S. de Marcos and J. R. Castillo, *Talanta*, 2001, **54**, 847.
2 D. Yao, A. G. Vlessidis and N. P. Evmiridis, *Anal. Chim. Acta*, 2002, **467**, 133.
3 A. K. Bhargava, H. Lal and C. S. Pundir, *J. Biochem. Biophys. Methods*, 1999, **39**, 125.
4 F. Zhang, X. Wang, S. Ai, Z. Sun, Q. Wan, Z. Zhu, Y. Xian, L. Jin, K. Yamamoto, J. Wang, T. Golden and P. Tuzhi, *Anal. Chem.*, 1987, **59**, 740–744.
5 F. Arslan, *Sensors*, 2008, **8**, 5492.
6 X. Y. Wang, T. Hagiwara and S. Uchiyama, *Anal. Chim. Acta*, 2007, **1**, 41.

7 D. Martinez-Perez, M. L. Ferrer and C. R. Mateo, *Anal. Biochem.*, 2003, **322**, 238.
8 J. Kan, X. Pan and C. Chen, *Biosens. Bioelectron.*, 2004, **19**, 1635.
9 A. Salimi, E. Sharif, A. Noorbakhs and S. Soltanian, *Biophys. Chem.*, 2007, **125**, 540.
10 J. Yang, L. C. Jiang, W. D. Zhang and S. Gunasekaran, *Talanta*, 2010, **82**, 25.
11 S. Saha, S. K. Arya, S. P. Singh, K. Sreenivas, B. D. Malhotra and V. Gupta, *Biosens. Bioelectron.*, 2009, **24**, 2040.
12 T. Ahuja, D. Kumar, V. K. Tanwar, V. Sharma, N. Singh and A. M. Biradar, *Thin Solid Films*, 2010, **519**, 1128.
13 S. M. U. Ali, N. H. Alvi, O. Nur, M. Willander and B. Danielsson, *Sens. Actuators, B*, 2011, **152**, 241.
14 C. W. Liao, J. C. Chou, T. P. Sun, S. K. Hsiung and J. H. Hsieh, *IEEE Trans. Biomed. Eng.*, 2006, **53**, 7.
15 F. F. Zhang, X. L. Wang, C. X. Li, X. H. Li, Q. Wan, Y. Z. Xian, L. T. Jin and K. Yamamoto, *Anal. Bioanal. Chem.*, 2005, **382**, 1368.
16 A. Sharma, M. Tomar and V. Gupta, *Sens. Actuators, B*, 2011, **156**, 743.
17 M. Batzill and U. Diebold, *Prog. Surf. Sci.*, 2005, **79**, 147.
18 D. Haridas, A. Chowdhuri, K. Sreenivas and V. Gupta, *Sens. Actuators, B*, 2011, **153**, 152.
19 F. F. Bentley, L. D. Smithson and A. L. Rozek, *Infrared Spectra and Characteristic Frequencies 700–300 cm^{-1}*, Interscience Publishers, London and Sydney, New York, 1968, (spectrum number: 1556)
20 D. E. Milligan and M. E. Jacox, *J. Chem. Phys.*, 1963, **38**, 2627.
21 Z. Matharu, P. Pandey, M. K. Pandey, V. Gupta and B. D. Malhotra, *Electroanalysis*, 2009, **21**, 1587.
22 A. Sharma, Z. Matharu, G. Sumana, P. R. Solanki, C. G. Kim and B. D. Malhotra, *Thin Solid Films*, 2010, **519**, 1213.
23 A. Kaushik, P. R. Solanki, A. A. Ansari, S. Ahmad and B. D. Malhotra, *Electrochem. Commun.*, 2008, **10**, 1364.
24 U. Yogeswaran and S. M. Chen, *Electrochim. Acta*, 2007, **52**, 5985.
25 S. Behera and C. Retna Raj, *Sens. Actuators, B*, 2007, **128**, 31.
26 S. Behera and C. Retna Raj, *Biosens. Bioelectron.*, 2007, **23**, 556.
27 S. B. Revin and S. A. John, *Bioelectrochemistry*, 2012, **88**, 22.
28 C. M. Zanon, N. Osvaldo, J. Oliveira and L. Caseli, *J. Colloid Interface Sci.*, 2012, **373**, 69.
29 K. Arora, G. Sumana, V. Saxena, R. K. Gupta, S. K. Gupta, J. V. Yakhmi, M. K. Pandey, S. Chand and B. D. Malhotra, *Anal. Chim. Acta*, 2007, **594**, 17.
30 J. Singh, P. Kalita, M. K. Singh and B. D. Malhotra, *Appl. Phys. Lett.*, 2011, **98**, 123702.
31 H. Chu, X. Wei, M. Wu, J. Yan and Y. Tu, *Sens. Actuators, B*, 2012, **163**, 247.
32 Y. C. Luo, J. S. Do and C. C. Liu, An amperometric uric acid biosensor based on modified Ir–C electrode, *Biosens. Bioelectron.*, 2006, **22**, 482.
33 R. Manjunatha, G. Shivappa, J. S. Melo, S. F. D'Souza and T. V. Venkatesha, *Sens. Actuators, B*, 2010, **145**, 643.
34 X. Liu, Y. Peng, X. Qu, S. Ai, R. Han and X. Zhu, *J. Electroanal. Chem.*, 2011, **654**, 72.
35 K. Arora, G. Sumana, V. Saxena, R. K. Gupta, S. K. Gupta, J. V. Yakhmi, M. K. Pandey, S. Chand and B. D. Malhotra, *Anal. Chim. Acta*, 2007, **594**, 17.
36 A. Salimi, H. MamKhezri and R. Hallaj, *Talanta*, 2006, **70**, 823.
37 P. Y. Chen, P. C. Nien, C. W. Hu and K. C. Ho, *Sens. Actuators, B*, 2010, **146**, 466.
38 C. Zhao, L. wan, Q. Wang, S. Liu and K. jiao, *Anal. Sci.*, 2009, **25**, 1013.